Theor Chem Acc (2004) 111:196–203
DOI 10.1007/s00214-003-0520-9

Theoretical
Chemistry Accounts

Regular article

An averaged solvent electrostatic potential from molecular dynamics study of the anomeric equilibrium of D-xylose in aqueous solution

I. Fdez. Galván, F.J. Olivares del Valle, M.E. Martín, M.A. Aguilar

Dpto Química-Física, Univ. de Extremadura, Avda de Elvas s/n, 06071, Badajoz, Spain

Received: 20 February 2003 / Accepted: 30 April 2003 / Published online: 5 December 2003

Abstract. We applied the free-energy perturbation method together with the averaged solvent electrostatic potential from molecular dynamics (ASEP/MD) method to study the anomeric equilibrium of D-xylose in aqueous solution. The level of calculation, 6-311G++(2d,2p) basis set and density functional theory, permits one to explain the main characteristics of the anomeric equilibrium of D-xylopyranose: in vacuo, the anomeric effect predominates and the α form is the stabler. In water, solvation leads to the β form being the stabler. A comparison between the performances of the ASEP/MD and polarizable continuum models is also presented.

Keywords: Solvent effects – QM/MM methods – ASEP/MD – Xylopyranose – Anomeric effect

Introduction

Effective Hamiltonian methods are now widely used in the study of molecules and processes in the liquid phase [1]. This kind of method focuses on a part of the system, the solute, which is described quantum mechanically, while the rest of the system, the solvent, is described in a simplified way. In this way, it is possible to get practically the same level of calculation and accuracy for molecules in solution as has already been achieved for molecules in vacuo. The effect of the solvent enters as an effective perturbation in the solute molecular Hamiltonian—hence its name. The different versions of the theory come from the different levels of description of the solvent. In the simplest models the solvent is described as a dielectric continuum [1, 2, 3, 4]. Pioneer works in this field were due to the groups of Tapia [4], Rivail [3], and Tomasi [1]. In general, continuum models take the solute to be inside a spherical or an ellipsoidal cavity, and a multipole expansion truncated at a certain order is employed in the description of the solute–solvent interaction. In the continuum version developed by the Tomasi group [1], known as the polarizable continuum model (PCM), the cavity is adapted to the molecular shape of the solute and the solvent perturbation is represented through a set of apparent charges placed on the cavity surface. In this way, it is not necessary to truncate the interaction potential. Continuum models have been successfully applied to the description of solvent effects on spectra [5], reactions [6], or molecular properties [7]. Their main limitation is that they neglect the microscopic structure of the solvent around the solute molecule. Because of this, many semicontinuum versions [1] have been developed where a small number of solvent molecules are explicitly included in the quantum region.

A major step forward in solvent-effect theories was represented by the use of quantum mechanics (QM)/molecular mechanics (MM) methods [8]. Here, the solvent is described by MM. When combined with simulation techniques [9] these methods permit one to obtain an adequate description of both the solute charge distribution and the solvent structure around it.

Most QM/MM methods combine a molecular dynamics (MD) simulation step with a quantum calculation, and hence it is necessary to perform as many quantum calculations as time steps in the MD simulation. An alternative strategy is to introduce the mean field (MF) approximation [10]. In this case, one alternates complete MD simulations and quantum calculations for the solute molecule in the presence of the average perturbation generated by the solvent. This approximation neglects the correlation between the solute polarization and the solvent structure around it, i.e., the solute charge distribution responds to the average perturbation, not to the instantaneous solvent configu-

Contribution to the Jacopo Tomasi Honorary Issue

Correspondence to: M. A. Aguilar
e-mail: maguilar@unex.es

ration. Previous studies [10] have shown that this correlation energy, known as the Stark component, represents less than 2% of the solute–solvent interaction energy and that its effect on the dipole moment is less than 1%. The main advantage associated with the use of the MF approximation is that it permits one to drastically reduce the number of quantum calculations to be performed, and hence it becomes possible to describe the quantum subsystem with computationally intensive ab initio wavefunctions. A MF theory where the solvent structure is obtained from integral theories has also been proposed [11].

In many chemical processes, a high-level description of the quantum subsystem is compulsory. Previous studies [12] of glucopyranose, for instance, have shown the importance of including diffuse functions and correlation energy to obtain a proper description of the conformational equilibrium in monosaccharides. In vacuo, the conformational energy surfaces of aldohexoses and aldopentoses are determined by the anomeric effect and the formation of intramolecular hydrogen bonds. In aqueous solution, the conformational analysis is complicated by the competition between intermolecular and intramolecular hydrogen bonds. In this kind of problem, where a high-level description of the solute must be combined with a detailed description of the solvent structure around it, it is especially well suited to the combined use of QM/MM theories and the MF approximation. As an example application, we here investigate structural aspects of the anomeric equilibrium of D-xylopyranose in water.

The outline of the paper is as follows. The details of the MF theory used are described in Sect. 2, with special attention being paid to the description of the optimization geometry algorithm based on the free-energy gradient method. The influence of the solvent on the solute geometry and charge distribution and on the solvent structure are analysed in Sect. 3. Lastly, some conclusions are drawn in Sect. 4.

Details of the computational scheme

We used a nontraditional QM/MM method that alternates MD and QM calculations in an iterative procedure (Fig. 1). The details of the method have been described in a number of publications [13, 14]. During the MD simulation, the geometry and charge distribution of the solute and solvent molecules are considered as fixed. From the MD data one obtains the averaged solvent electrostatic potential (ASEP), which is then introduced as a perturbation into the solute molecular Hamiltonian. In order to facilitate its use with standard quantum programs, the ASEP is represented by a set of charges obtained in the following way:

1. All the charges belonging to solvent molecules that, in any of the MD configurations, lie within a sphere of radius R are included. R is chosen in such a way that it includes the first solvation shell. The value of any charge is divided by the number of solvent configurations included in the calculation of the ASEP.
2. Next, a second set of charges is obtained by a least-squares fit to the values of the electrostatic potential originating from the solvent molecules lying beyond the first solvation shell.

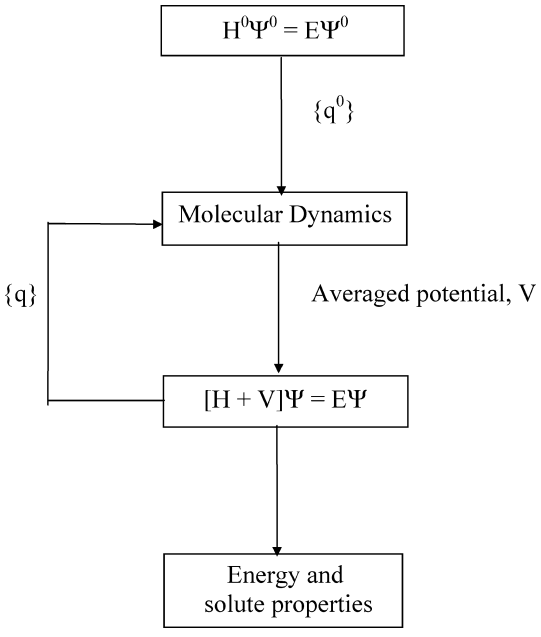

Fig. 1. Flow chart of the coupled averaged solvent electrostatic potential from molecular dynamics model

By introducing the ASEP into the solute Schrödinger equation we get a new solute charge distribution and geometry that serve as inputs for a new MD calculation. At each step the new geometry is obtained from the old one using the rational function optimization method [15]:

$$q_{k+1} = q_k + \Delta q_k \ , \tag{1}$$

where Δq_k gives the correction to the molecular geometry and is calculated by diagonalizing the augmented Hessian matrix. The force, which is the spatial derivative of the free-energy surface [16], G, is approximated as [14]

$$F(r) = -\frac{\partial G(r)}{\partial r} = -\left\langle \frac{\partial V}{\partial r} \right\rangle \approx -\frac{\partial \langle V \rangle}{\partial r} \ , \tag{2}$$

where V is the potential energy which is the sum of intramolecular and intermolecular contributions and the brackets denote a statistical average. As one can see, following the spirit of the MF approximation, we replace the average value of the gradient by the gradient of the average configuration. Using the same approximation, the Hessian is

$$H = \frac{\partial^2 \langle V \rangle}{\partial r \partial r} \ , \tag{3}$$

where we have furthermore neglected the terms associated with the thermal fluctuations of the gradient.

The ASEP/MD process terminates when convergence in the solute charges and in the solute energy is reached. The charges that represent the D-xylopyranose molecule during the MD were obtained from the wavefunction of the solute molecule in solution by using the CHELPG method [17].

All quantum calculations were performed with the program Gaussian 98 [18]. The 6-311G + + G(2d,2p) basis set [19] was used. The use of an extended basis set is necessary to adequately describe the intramolecular hydrogen bonds. The energy and wavefunctions were calculated using density functional theory with the Becke three-parameter Lee–Yang–Parr functional [20].

The MD calculations were performed using the program MOLDY [21]. One xylose molecule in its pyranose conformation surrounded by 214 TIP3P [22] water molecules was simulated at a

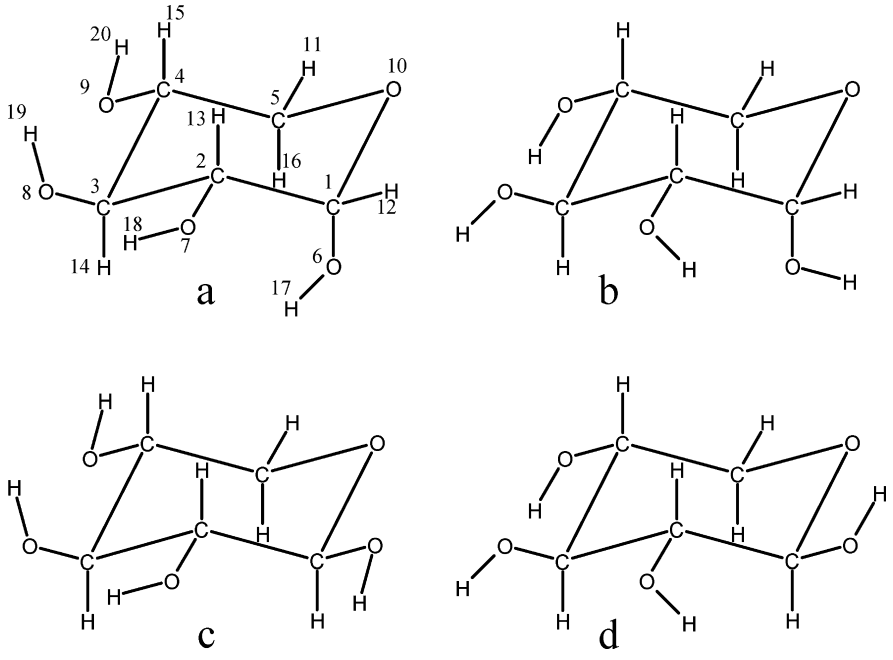

Fig. 2. Four conformers of D-xylopyranose: **a** clockwise α-xylopyranose, **b** counterclockwise α-xylopyranose, **c** clockwise β-xylopyranose, **d** counterclockwise β-xylopyranose

fixed intramolecular geometry by combining Lennard-Jones interatomic interactions with electrostatic interactions in a cubic simulation box of side 18.8 Å. The pyranose–water Lennard-Jones potential parameters were taken from Ref. [23]. Periodic boundary conditions were applied, and spherical cutoffs were used to truncate the molecular interactions at 9.0 Å. A time step of 0.5 fs was used. The electrostatic interaction was calculated with the Ewald method. The temperature was fixed at 298 K by using a Nosé–Hoover [24] thermostat. Each MD calculation simulation was run for 250 000 time steps (50 000 equilibration, 200 000 production).

Having obtained the final charges for the two anomers with the ASEP/MD method, we performed free-energy simulations in a canonical ensemble (N,V,T) to transform one of the two anomers into the other. To the free energy thus obtained, which is completely classical, one adds the difference in the internal energies of the two solutes calculated with ab initio methods:

$$\Delta E^{\text{internal}} = <\Psi_\beta \left| \bar{\mathbf{H}}^0 \right| \Psi_\beta > - <\Psi_\alpha \left| \bar{\mathbf{H}}^0 \right| \Psi_\alpha > \ , \qquad (4)$$

where Ψ_β and Ψ_α are the wavefunctions in solution of the two anomers considered, and $\mathbf{H}^0$ is the gas-phase solute molecular Hamiltonian. The solution free-energy simulations were obtained using the free-energy perturbation method [25] with both single and dual topology. The coupling parameter, λ, was divided into 20 equally distributed intervals of 0.05 units.

Results and discussion

In solution, xylose cyclizes to produce five-membered (furanose form) or six-membered (pyranose form) rings, the pyranose form being the preferred form in solution. On cyclization, the achiral C1 carbon atom of an aldopentose becomes chiral. Depending on the position, axial or equatorial, of the OH group generated by cyclization, there are two sterochemical species, anomers α or β, for xylopyranose. Furthermore, for the isolated monomer, the hydroxyl groups prefer to orient in such a way as to yield a cooperative hydrogen bonding that is as efficient as possible. Two of these arrangements of the intramolecular hydrogen bonds are preferred: clockwise or counterclockwise. The four structures are displayed in Fig. 2. In the gas phase, Table 1, the counterclockwise orientation is preferred by 2.20 kcal/mol in the α anomer and by 3.59 kcal/mol in the β anomer. In vacuo, the α anomer is only slightly stabler than the β anomer (by less than 1 kcal/mol). In solution, the intramolecular hydrogen bonds can be broken and substituted by intermolecular hydrogen bonds with the water molecules, and the relative stability of the two anomers can be reversed.

We begin by analysing the changes introduced by the solvent in the geometry of the two anomers, both in their counterclockwise conformation. The root-mean-square change of the gradient on the free-energy surface during the optimization of the β anomer in aqueous solution obtained with 125 (25 + 100)-ps simulations is shown in Fig. 3. Convergence is reached in 5–6 cycles. From this point, the gradient begins to fluctuate around a root-mean-square gradient value of about 0.0005 hartree/bohr. This value is similar to that obtained in other compounds using the same technique, and is somewhat lower than the values obtained by other authors [16] who combined QM/MM and free-energy gradient methods but did not introduce the MF approximation.

Table 1. Relative stability of the different conformations of xylopyranose

	α-Xylopyranose		β-Xylopyranose	
	Counterclockwise	Clockwise	Counterclockwise	Clockwise
Energy (au)	–572.854188	–572.850679	–572.852800	–572.847073
ΔE (kcal/mol)	0.0	2.20	0.87	4.46

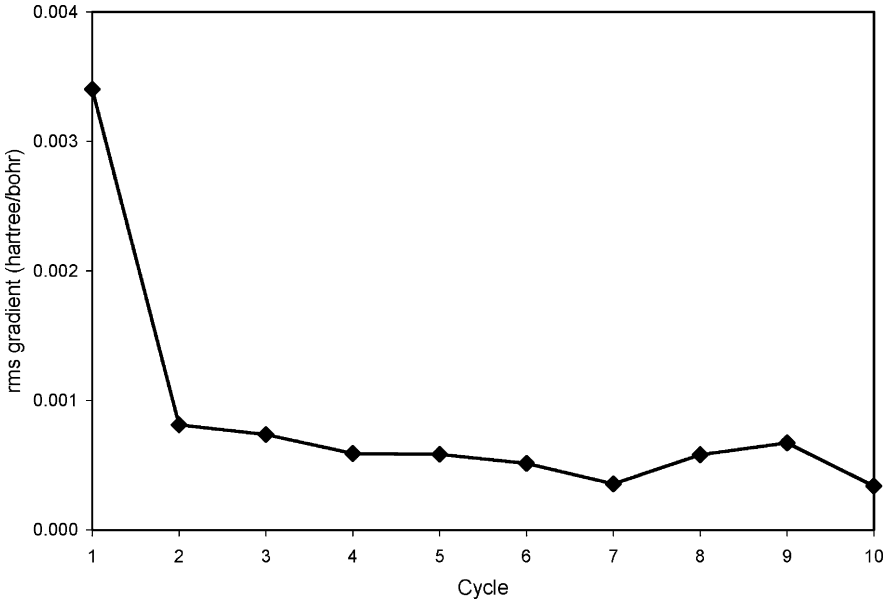

Fig. 3. Gradient root-mean-square (*rms*) change in free-energy surface of counterclockwise β-xylopyranose in aqueous solution

The evolution of the polarization free energy during the optimization procedure, i.e., the change in the solute–solvent interaction free energy when the solute charge distribution passes from its in vacuo values to the final charge distribution in solution, is shown in Fig. 4. As before, convergence is reached in 5–6 cycles, then ΔG begins to fluctuate. The free energies were calculated by the free-energy perturbation method [25]. The final values of the energy (and of the rest of the properties) were obtained by averaging the results of the last five cycles. The behaviour of the gradient and free energy for the α anomer is completely similar and is not displayed here.

In general, the variations in the geometry induced by the solvent, Table 2, are small. The C–C and C–H distances decrease by about 0.005 and 0.008 Å, respectively. In contrast, the C–O hydroxyl distances increase probably owing to the participation of the oxygen atom in intermolecular hydrogen bonds. The largest difference between the two anomers appears in the C1–O anomeric distance: in the β anomers it does not vary with respect to the in vacuo value, but in the α anomer it decreases by almost 0.01 Å. In angles, the largest variation appears in the COH angles, which increase by about 2.5°.

A summary of the thermodynamic results is given in Table 3. For comparison, we also give the results obtained with the PCM as implemented in Gaussian [18] and with a scale factor for the radius of each atomic sphere of 1.2. This model erroneously predicts that solution favours the α anomers. In fact, the solvation free energy is 1.1 kcal/mol larger in the α anomers than

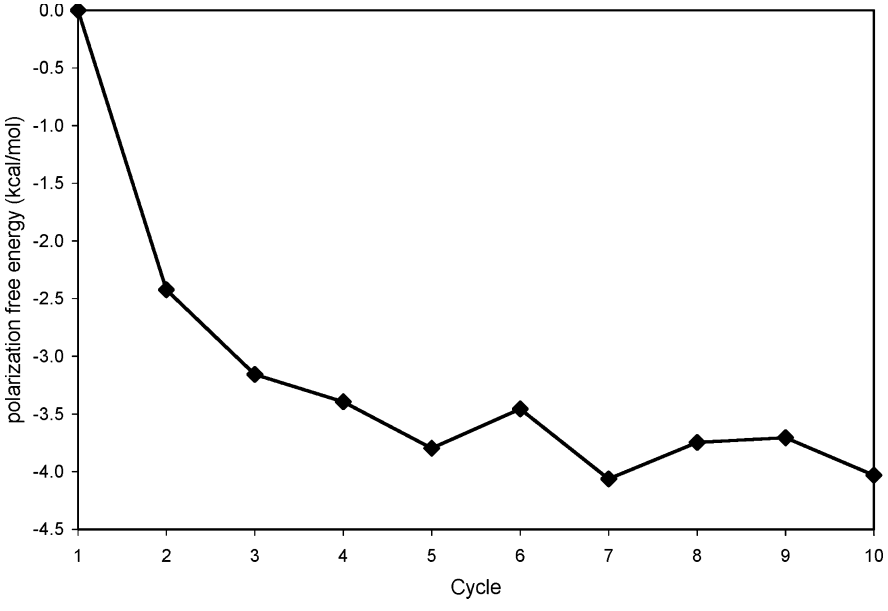

Fig. 4. Polarization free-energy change of counterclockwise β-xylopyranose in aqueous solution during the optimization procedure

Table 2. Optimized geometry for the two anomers in vacuo and insolution. Distances in angstroms, angles in degrees

	α-D-Xylopyranose		β-D-Xylopyranose	
	In vacuo	In solution	In vacuo	In solution
C1–C2	1.536	1.529	1.530	1.526
C2–C3	1.531	1.527	1.523	1.521
C3–C4	1.524	1.519	1.527	1.522
C4–C5	1.528	1.523	1.532	1.525
C5–O10	1.436	1.433	1.427	1.428
C1–O10	1.407	1.415	1.419	1.421
C1–O6	1.419	1.408	1.395	1.394
C2–O7	1.421	1.422	1.420	1.423
C3–O8	1.421	1.425	1.420	1.423
C4–O9	1.417	1.425	1.416	1.421
C1–H12	1.097	1.088	1.107	1.095
C2–H13	1.095	1.089	1.100	1.093
C3–H14	1.102	1.093	1.103	1.095
C4–H15	1.103	1.093	1.102	1.093
C5–H11	1.092	1.085	1.092	1.085
C5–H16	1.097	1.091	1.102	1.094
O6–H17	0.966	0.964	0.967	0.965
O7–H18	0.970	0.966	0.967	0.964
O8–H19	0.968	0.965	0.968	0.964
O9–H20	0.968	0.965	0.968	0.965
C1–O6–H17	108.2	109.5	108.2	109.7
C2–O7–H18	105.6	108.1	106.9	109.0
C3–O8–H19	106.3	108.7	106.7	109.3
C4–O9–H20	106.1	108.9	106.1	109.1

in the β ones. In contrast, the ASEP/MD predicts the correct trend: in solution the stabler form is the β anomer. Given that in vacuo the anomeric effect favours the α anomer, the greater stability in solution of the β anomer must be due to a more favourable solvent interaction term. In the calculation of the free energy, excellent agreement between the two simulations, direct and reverse, is found. This fact shows the good precision of the simulations. The two free-energy methods used, single and dual topology, yield very similar results. Taking as a final value the average value of the direct and reverse calculations (0.5 and 0.7 kcal/mol for the dual and single topology methods, respectively) one obtains a relative stability that agrees very well with the experimental value [26], 0.4 kcal/mol.

That the solvation term favours the β anomer is confirmed by the results obtained from the separate ASEP/MD simulations of the two anomers, Table 4. In the two cases considered, the electrostatic component makes the largest contribution to the interaction energy, being more favourable to the β anomer by almost

Table 3. Calculated anomeric free energy differences for D-xylopyranose

Transformation direction	Polarizable continuum model	Free-energy perturbation		Experimental
		Single topology	Dual topology	
$\alpha \rightarrow \beta$		−0.9	−0.5	
$\beta \rightarrow \alpha$		−0.7	−0.7	
Mean	2.0	−0.8	−0.6	−0.4

Table 4. Solute–solvent interaction energy and its components (kcal/mol)

	α-Xylopyranose		β-Xylopyranose	
	First cycle[a]	Final average[b]	First cycle[a]	Final average[b]
μ (D)	2.15	3.0	1.94	2.37
E_{elect}	−23.9	–34.1	–26.3	–37.1
E_{dist}	1.3	2.5	1.46	2.7
E_{LJ}	–11.1	–8.8	–10.8	–7.8
E_{int}[c]	–33.7	–40.4	–35.26	–42.2

[a]The dipole moment in the first cycle is the in vacuo value
[b]The average values are calculated with the last five cycles of the averaged solvent electrostatic potential frommolecular dynamics procedure
[c]The solute–solvent and inter action energy is calculated as the sum of the three previous contributions, where E_{elect} is the electrostatic component that includes the solute polarization, E_{LJ} is the Lennard-Jones component, and E_{dist} is the distortion energy or energy spent in polarizing the solute

3 kcal/mol. The interaction energies do not correlate with the dipole moment. In fact, the largest interaction energy corresponds to the β anomer, which has the lower dipole moment of the two anomers both in vacuo and in solution. The solvation of monosaccharides is clearly dominated by intermolecular hydrogen bonds, and continuum models cannot take this effect into account. Because of this, the PCM predicts greater solvation in the α anomer. The rest of the components favour the α form, and as a consequence the differences in the final solute–solvent interaction energy favour the β anomer by 1.8 kcal/mol. The β anomer is the stabler even if one uses the in vacuo charge distribution, i.e., if one does not permit the molecules to polarize as a consequence of the potential reaction generated by the solvent. In fact, if the in vacuo charges are used in the MD calculation then the difference of energy between the two anomers is 2.36 kcal/mol favourable to the β anomer.

During solution, the two anomers undergo strong polarization, which is greater in the α anomer: the induced dipole moments represent 22% of the in vacuo values for the β anomer and almost 37% in the α anomer. The CHELPG charges in vacuo and in solution are given in Table 5. In general, the two anomers have a similar charge distribution except on the C1 atom, where, in vacuo, the charge in the β anomer is almost twice that in the α anomer. This difference is somewhat reduced in solution. There also exist appreciable differences in the charges in solution on the anomeric oxygen and on the hydroxyl oxygen bonded to C2.

The oxygen (anomeric)–oxygen (water) radial distribution functions (RDFs) for the two anomers are shown in Fig. 5. The first peak is higher in the β anomer than in the α anomer, indicating a preferential solvation of the β anomer. This contrasts with what was recently found with an ab initio MD calculation of glucose [27], where the RDF of the β anomer was broader and lower than the RDF of the α anomer. The study of the coordination numbers of the anomeric oxygen also confirms the preferential solvation of the β anomer—4.43 for the

Table 5. CHELPG charge distribution of the two anomers

	α-D-Xylopyranose		β-D-Xylopyranose	
	In vacuo	In solution	In vacuo	In solution
C1	0.233	0.343	0.464	0.474
C2	0.262	0.200	0.188	0.189
C3	0.132	0.293	0.199	0.298
C4	0.348	0.293	0.324	0.321
C5	0.169	0.237	0.176	0.176
O6	−0.641	−0.687	−0.659	−0.742
O7	−0.627	−0.711	−0.679	−0.803
O8	−0.670	−0.783	−0.704	−0.805
O9	−0.709	−0.836	−0.714	−0.833
O10	−0.480	v0.573	−0.517	−0.572
H11	0.069	0.066	0.076	0.093
H12	0.080	0.078	–0.016	0.029
H13	0.057	0.073	0.059	0.081
H14	0.051	0.049	0.029	0.030
H15	−0.007	0.029	0.004	0.028
H16	0.042	0.039	0.015	0.035
H17	0.442	0.480	0.429	0.489
H18	0.385	0.429	0.425	0.496
H19	0.422	0.476	0.454	0.504
H20	0.440	0.503	0.446	0.510

α anomer and 5.43 for the β anomer. The O–O RDF for the hydroxyl group of C3 is shown in Fig. 6. The differences between the two anomeric forms are minimal, with the first peak being slightly higher in the α anomer. The rest of the hydroxyl groups in xylopyranose have similar RDFs. The coordination numbers in this case are now 3.46 for the two anomers. For all these reasons, it seems clear that the relative stabilization of the β anomers in solution is related to a better solvation of the anomeric hydroxyl group, the influence of the rest of the molecule being minimal.

We finish by noting that there are remarkable differences between the RDF shown in Fig. 6 and those reported in Ref. [28]. Our O–O8 RDF peaks are far lower. Our results in this case agree better with those obtained by Molteni and Parrinello [27] using ab initio MD.

Conclusions

We have demonstrated how, when combined with extended basis sets and correlated ab initio methods, the ASEP/MD method permits one to explain the main characteristics of the anomeric equilibrium of D-xylopyranose. In vacuo, the anomeric effect predominates and the α form is the stabler. In water, solvation favours the β form, which becomes the stabler form. From the analysis of the O–O RDF functions and of the estimated coordination numbers it seems clear that there is a difference in the water structure around the anomeric hydroxyl group which increases hydrogen bonding in the β anomer. Our study predicts O–O RDFs that differ from those obtained by other authors. They also differ from a recent ab initio MD study [27] of glucose in that first peak of the oxygen (anomeric)–oxygen (water) is higher in the β anomer than in the α anomer, indicating a preferential solvation of the β anomer. However, we do not find such high peaks for the O–O8 RDF as do Liu and Brady [28], and in this respect our result resembles more closely the findings of Molteni and Parrinello.

Unlike previous studies, the present ASEP/MD simulations assign different charges to the two anomers and permit the solutes to polarize in response to the reaction field generated by the solvent. While the two anomeric forms undergo strong polarization in aqueous solution, this is not the factor that explains the greater stability of the β form. Indeed, the α form is more polarized in solution. The main factor that determines the stability of the β form is the difference in the in vacuo charge distribution of the two anomers, more specifically, the charges on the carbon and anomeric hydroxyls.

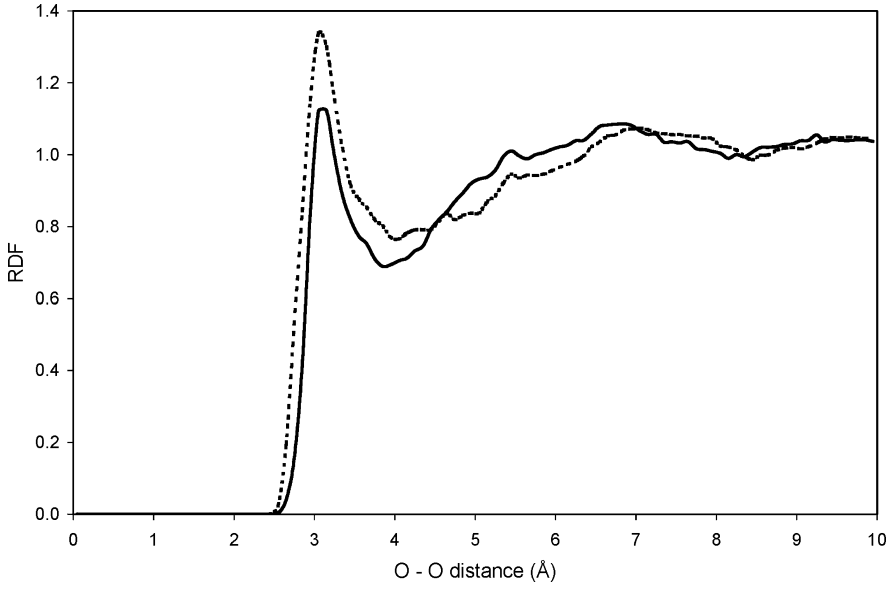

Fig. 5. Oxygen (water)–oxygen (anomeric) radial distribution function (*RDF*) for anomers α (*full line*) and β (*dashed line*)

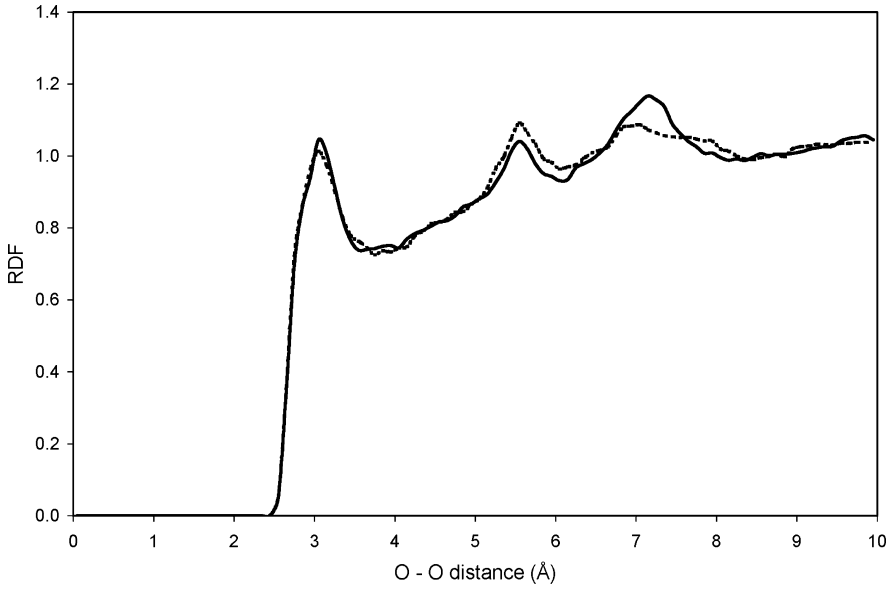

Fig. 6. Oxygen (water)–oxygen (bonded to C3) RDF for anomers α (*full line*) and β (*dashed line*)

Acknowledgements. This research was sponsored by the Dirección General de Investigación Científica y Técnica (project no. BQU2000-0243) and by the Consejería de Educación Ciencia y Tecnología de la Junta de Extremadura (project no. 2PR01A010).

References

1. (a) Tomasi J, Bonaccorsi R, Cammi R, Olivares del Valle FJ (1991) J Mol Struct (THEOCHEM) 234:401; (b) Tomasi J, Persico M (1994) Chem Rev 94:2027
2. Cramer CJ, Truhlar CJ (1995) In: Lipkowitz KB, Boyd DB (eds) Reviews in computational chemistry, vol VI. VCH, New York, p 1
3. Rivail JL, Rinaldi D (1995) In: Leszczynski J (ed) Computational chemistry: review of current trends. World Scientific, Singapore, pp
4. Tapia O, Goschinski O (1975) Mol Phys 29:1653
5. (a) Aguilar MA, Olivares del Valle FJ, Tomasi J (1993) J Chem Phys 98:7375; (b) Cossi M, Barone V (2000) J Phys Chem A 104:10614; (c) Mennucci B, Cammi R, Tomasi J (1998) J Chem Phys 109:2798
6. (a) Bonnacorsi R, Cimiraglia R, Tomasi J, Miertus S (1983) J Mol Struct (THEOCHEM) 94:11; (b) Lee S, Hynes JT (1988) J Chem Phys 88:6953; (c) Karlström G (1988) J Phys Chem 92:1315; (d) Alemán C, Maseras F, Lledós A, Duran M, Bertrán J (1989) J Phys Org Chem 2:611
7. (a) Ruiz López MF, Rinaldi D, Rivail J-L (1986) J Mol Struct (THEOCHEM) 148:61; (b) Cammi R, Cossi M, Tomasi J (1996) J Chem Phys 104:4611; (c) Cammi R, Mennucci B, Tomasi J (1998) J Phys Chem A 102:870
8. (a) Warshel A, Levitt M (1976) J Mol Biol 103:227; (b) Singh UC, Kollman PA (1986) J Comput Chem 7:718; (c) Field MJ, Bash PA, Karplus M (1990) J Comput Chem 11:700; (d) Luzhkov V, Warshel A (1992) J Comput Chem 13:199; (e) Gao J (1996) In: Lipkowitz KB, Boyd DB (eds) Reviews in computational chemistry, vol 7. VCH, New York, p 119
9. (a) Allen MP, Tildesley DJ (1987) Computer simulation of liquids. Oxford University Press, London; (b) Frenkel D, Smit B. (2002) Understanding molecular simulations, 2nd edn. Academic, New York
10. (a) Tapia O (1991) In: Maksic ZB (ed) Theoretical treatment of large molecules and their interactions, vol 4. Springer, Berlin Heidelberg New York, p 435; (b) Sánchez ML, Martín ME, Fdez Galván I, Olivares del Valle FJ, Aguilar MA (2002) J Phys Chem B 106:4813
11. (a) Ten-no S, Hirata F, Kato S (1993) Chem Phys Lett 214:391; (b) Ten-no S, Hirata F, Kato S (1994) J Chem Phys 100:7443; (c) Kawata M, Ten-no S, Kato S, Hirata F (1995) Chem Phys 240:199; (d) Kawata M, Ten-no S, Kato S, Hirata F (1996) J Phys Chem 100:1111; (e) Kinoshita M, Okamoto Y, Hirata F (1997) J Comput Chem 18:1320; (f) Akiyama R, Hirata F (1998) J Chem Phys 108:4904; (g) Sato H, Kovalenco A, Hirata F (2000) J Chem Phys 112:9463
12. Lii J-H, Ma B, Allinger NL (1999) J Comput Chem 20:1593
13. (a) Sánchez ML, Aguilar MA, Olivares del Valle FJ (1997) J Comput Chem 18:313; (b) Martín ME, Sánchez ML, Olivares del Valle FJ, Aguilar MA (2000) J Chem Phys 113:6308; (c) Sánchez ML, Martín ME, Aguilar MA, Olivares del Valle FJ (2000) J Comput Chem 21:705; (d) Martín ME, Sánchez ML, Olivares del Valle FJ, Aguilar MA (2002) J Chem Phys 116:1613; (e) Sánchez ML, Martín ME, Fdez Galván I, Olivares del Valle FJ, Aguilar MA (2002), J Phys Chem B 106:4813
14. Fdez Galván I, Sánchez ML, Martín ME. Olivares del Valle FJ, Aguilar MA (2003) J Chem Phys 118:255
15. Prat-Resina X, García-Viloca M, Monard G, González-Lafont A, Lluch JM, Bofill JM, Anglada JM (2002) Theor Chem Acc 107:147
16. (a) Okuyama-Yoshida N, Nagaoka M, Yamabe T (1998) Inte J Quantum Chem 70:95; (b) Okuyama-Yoshida N, Kataoka K, Nagaoka M, Yamabe T (2000) J Chem Phys 113:3519; (c) Hirao H, Nagae Y, Nagaoka M (2001) Chem Phys Lett 348:350
17. (a) Chirlian LE, Francl MM (1987) J Comput Chem 8:894; (b) Breneman CM, Wiberg KB (1990) J Comput Chem 11:316
18. Frisch MJ, Trucks GW, Schlegel HB, Scuseria GE, Robb MA, Cheeseman JR, Zakrzewski VG, Montgomery JA Jr, Stratmann RE, Burant JC, Dapprich S, Millam JM, Daniels AD, Kudin KN, Strain MC, Farkas O, Tomasi J, Barone V, Cossi M, Cammi R, Mennucci B, Pomelli C, Adamo C, Clifford S, Ochterski J, Petersson GA, Ayala PY, Cui Q, Morokuma K, Malick DK, Rabuck AD, Raghavachari K, Foresman JB, Cioslowski J, Ortiz JV, Baboul AG, Stefanov BB, Liu G, Liashenko A, Piskorz P, Komaromi I, Gomperts R, Martin RL, Fox DJ, Keith T, Al-Laham MA, Peng CY, Nanayakkara A, Gonzalez C, Challacombe M, Gill PMW, Johnson B, Chen W, Wong MW, Andres JL, Gonzalez C, Head-Gordon M, Replogle ES, Pople JA (1998) Gaussian 98. Gaussian, Pittsburgh, PA
19. (a) McLean AD, Chandler GS (1980) J Chem Phys 72:5639; (b) Krishnan R, Binkley JS, Seeger R, Pople JA (1980) J Chem Phys 72:650
20. Becke AD (1993) J Chem Phys 98:5648

21. Refson K (1996) Moldy user's manual revision 2.10. University of Oxford, Oxford,ftp://ftp.earth.ox.ac.uk/pub
22. Jorgensen WL, Chandrasekhar J, Madura JD, Impey RW, Klein ML (1983) J Chem Phys 79:926
23. Sookhee N, Giammona A, Field M, Brady JW (1988) Carbohydr Res 180:207
24. Hoover WG (1985) Phys Rev A 31:1695
25. (a) Zwanzig RW (1954) J Chem Phys 22:1420; (b) Singh UC, Brown FK, Bash PA, Kollman PA (1987) J Am Chem Soc 109:1607
26. Höög C, Widmalm G (2001) J Phys Chem B 105:6375
27. Molteni C, Parrinello M (1998) J Am Chem Soc 120:2168
28. (a) Schmidt RK, Karplus M, Brady JW (1996) J Am Chem Soc 118:541; (b) Liu Q, Brady JW (1996) J Am Chem Soc 118:12276; (c) Liu Q, Brady JW (1997) J Phys Chem B 101:1317